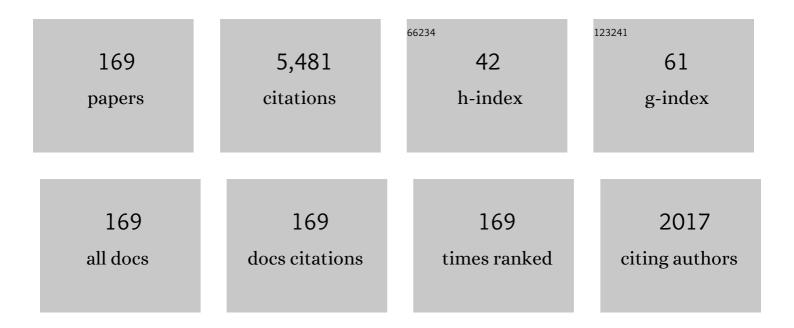
List of Publications by Year in descending order

Source: https://exaly.com/author-pdf/7753372/publications.pdf Version: 2024-02-01



HONG-BO GUO

#	Article	IF	CITATIONS
1	Microstructure and thermo-physical properties of yttria stabilized zirconia coatings with CMAS deposits. Journal of the European Ceramic Society, 2011, 31, 1881-1888.	2.8	164
2	Cyclic oxidation of β-NiAl with various reactive element dopants at 1200°C. Corrosion Science, 2013, 66, 125-135.	3.0	164
3	Microstructure and Thermal Properties of Plasma Sprayed Thermal Barrier Coatings from Nanostructured YSZ. Journal of Thermal Spray Technology, 2010, 19, 1186-1194.	1.6	126
4	Microstructures and Properties of Plasma-Sprayed Segmented Thermal Barrier Coatings. Journal of the American Ceramic Society, 2006, 89, 1432-1439.	1.9	119
5	High temperature oxidation behavior of hafnium modified NiAl bond coat in EB-PVD thermal barrier coating system. Thin Solid Films, 2008, 516, 5732-5735.	0.8	118
6	Thermophysical properties of Yb2O3 doped Gd2Zr2O7 and thermal cycling durability of (Gd0.9Yb0.1)2Zr2O7/YSZ thermal barrier coatings. Journal of the European Ceramic Society, 2014, 34, 1255-1263.	2.8	113
7	Lanthanum–titanium–aluminum oxide: A novel thermal barrier coating material for applications at 1300°C. Journal of the European Ceramic Society, 2011, 31, 1677-1683.	2.8	108
8	Plasma-sprayed La2Ce2O7 thermal barrier coatings against calcium–magnesium–alumina–silicate penetration. Journal of the European Ceramic Society, 2014, 34, 2553-2561.	2.8	103
9	Microstructure and mechanical properties of yttria stabilized zirconia coatings prepared by plasma spray physical vapor deposition. Ceramics International, 2015, 41, 8305-8311.	2.3	98
10	Thermal shock resistance and mechanical properties of La2Ce2O7 thermal barrier coatings with segmented structure. Ceramics International, 2009, 35, 2639-2644.	2.3	97
11	Effect of co-doping of two reactive elements on alumina scale growth of β-NiAl at 1200°C. Corrosion Science, 2014, 88, 197-208.	3.0	83
12	Effect of Dy on oxide scale adhesion of NiAl coatings at 1200 °C. Corrosion Science, 2011, 53, 2228-2232.	3.0	81
13	Effect of Sm, Gd, Yb, Sc and Nd as reactive elements on oxidation behaviour of β-NiAl at 1200°C. Corrosion Science, 2014, 78, 369-377.	3.0	78
14	Improved cyclic oxidation resistance of electron beam physical vapor deposited nano-oxide dispersed β-NiAl coatings for Hf-containing superalloy. Corrosion Science, 2010, 52, 1440-1446.	3.0	77
15	Microstructure, hardness and corrosion behaviour of Ti/TiN multilayer coatings produced by plasma activated EB-PVD. Surface and Coatings Technology, 2014, 258, 102-107.	2.2	77
16	Influence of partial substitution of Sc2O3 with Gd2O3 on the phase stability and thermal conductivity of Sc2O3-doped ZrO2. Ceramics International, 2013, 39, 3447-3451.	2.3	72
17	Microstructure, thermal conductivity and thermal cycling behavior of thermal barrier coatings prepared by plasma spray physical vapor deposition. Surface and Coatings Technology, 2015, 276, 424-430.	2.2	72
18	Effect of Mo, Ta, and Re on high-temperature oxidation behavior of minor Hf doped β-NiAl alloy. Corrosion Science, 2016, 102, 222-232.	3.0	72

#	Article	IF	CITATIONS
19	Improvement on the phase stability, mechanical properties and thermal insulation of Y2O3-stabilized ZrO2 by Gd2O3 and Yb2O3 co-doping. Ceramics International, 2013, 39, 9009-9015.	2.3	68
20	Protectiveness of Pt and Gd2Zr2O7 layers on EB-PVD YSZ thermal barrier coatings against calcium–magnesium–alumina–silicate (CMAS) attack. Ceramics International, 2015, 41, 11662-11669.	2.3	67
21	Cyclic oxidation and interdiffusion behavior of a NiAlDy/RuNiAl coating on a Ni-based single crystal superalloy. Corrosion Science, 2011, 53, 2721-2727.	3.0	66
22	Microstructures of Yttria-Stabilized Zirconia Coatings by Plasma Spray-Physical Vapor Deposition. Journal of Thermal Spray Technology, 2015, 24, 534-541.	1.6	65
23	Thermal cycling behavior of La2Ce2O7/8YSZ double-ceramic-layer thermal barrier coatings prepared by atmospheric plasma spraying. Surface and Coatings Technology, 2010, 204, 3366-3370.	2.2	64
24	Degradation of EB-PVD thermal barrier coatings caused by CMAS deposits. Progress in Natural Science: Materials International, 2012, 22, 461-467.	1.8	63
25	Wetting, infiltration and interaction behavior of CMAS towards columnar YSZ coatings deposited by plasma spray physical vapor. Journal of the European Ceramic Society, 2018, 38, 3564-3572.	2.8	60
26	Deposition mechanisms of yttria-stabilized zirconia coatings during plasma spray physical vapor deposition. Ceramics International, 2016, 42, 5530-5536.	2.3	58
27	Novel thermal barrier coatings repel and resist molten silicate deposits. Scripta Materialia, 2019, 163, 71-76.	2.6	56
28	Thermo-Physical Properties and Thermal Shock Resistance of Segmented La2Ce2O7/YSZ Thermal Barrier Coatings. Journal of Thermal Spray Technology, 2009, 18, 665-671.	1.6	55
29	Diffusion barrier behaviors of (Ru,Ni)Al/NiAl coatings on Ni-based superalloy substrate. Intermetallics, 2011, 19, 191-195.	1.8	53
30	The role of Dy and Hf doping on oxidation behavior of two-phase (γ′ + β) Ni–Al alloys. Corrosion Science, 2015, 98, 699-707.	3.0	53
31	Structural evolution and thermal conductivities of (Gd1â^xYbx)2Zr2O7 (x=0, 0.02, 0.04, 0.06, 0.08, 0.1) ceramics for thermal barrier coatings. Ceramics International, 2015, 41, 12621-12625.	2.3	53
32	Thermal cycling behavior and failure mechanism of LaTi2Al9O19/YSZ thermal barrier coatings exposed to gas flame. Surface and Coatings Technology, 2011, 205, 4291-4298.	2.2	52
33	Cyclic oxidation and diffusion barrier behaviors of oxides dispersed NiCoCrAlY coatings. Journal of Alloys and Compounds, 2010, 502, 411-416.	2.8	51
34	High-temperature oxidation and hot-corrosion behaviour of EB-PVD β-NiAlDy coatings. Corrosion Science, 2011, 53, 1050-1059.	3.0	50
35	NiAlHf/Ru: Promising bond coat materials in thermal barrier coatings for advanced single crystal superalloys. Corrosion Science, 2014, 78, 304-312.	3.0	50
36	Microstructural, mechanical and oxidation features of NiCoCrAlY coating produced by plasma activated EB-PVD. Applied Surface Science, 2013, 274, 144-150.	3.1	49

#	Article	lF	CITATIONS
37	High-temperature oxidation behavior of minor Hf doped NiAl alloy in dry and humid atmospheres. Corrosion Science, 2013, 75, 337-344.	3.0	48
38	Thermo-physical and thermal cycling properties of plasma-sprayed BaLa2Ti3O10 coating as potential thermal barrier materials. Surface and Coatings Technology, 2009, 204, 691-696.	2.2	47
39	Hot-corrosion behavior of a La2Ce2O7/YSZ thermal barrier coating exposed to Na2SO4+V2O5 or V2O5 salt at 900°C. Ceramics International, 2015, 41, 6604-6609.	2.3	47
40	Microstructural characterization of PS-PVD ceramic thermal barrier coatings with quasi-columnar structures. Surface and Coatings Technology, 2017, 311, 199-205.	2.2	47
41	Influence of Gd2O3 and Yb2O3 Co-doping on Phase Stability, Thermo-physical Properties and Sintering of 8YSZ. Chinese Journal of Aeronautics, 2012, 25, 948-953.	2.8	46
42	Precipitation phases in the nickel-based superalloy DZ 125 with YSZ/CoCrAlY thermal barrier coating. Journal of Alloys and Compounds, 2011, 509, 8542-8548.	2.8	44
43	Effect of Sintering on Thermal Conductivity and Thermal Barrier Effects of Thermal Barrier Coatings. Chinese Journal of Aeronautics, 2012, 25, 811-816.	2.8	43
44	Comparative study on effect of oxide thickness on stress distribution of traditional and nanostructured zirconia coating systems. Ceramics International, 2013, 39, 475-481.	2.3	42
45	Hot Corrosion Behavior of Double-ceramic-layer LaTi2Al9O19/YSZ Thermal Barrier Coatings. Chinese Journal of Aeronautics, 2012, 25, 137-142.	2.8	41
46	Evaluation of plasma sprayed YSZ thermal barrier coatings with the CMAS deposits infiltration using impedance spectroscopy. Progress in Natural Science: Materials International, 2012, 22, 40-47.	1.8	41
47	Calcium-magnesium-alumina-silicate (CMAS) resistant Ba2REAlO5 (RE = Yb, Er, Dy) ceramics for thermal barrier coatings. Journal of the European Ceramic Society, 2017, 37, 4991-5000.	2.8	41
48	Thermal Cycling Behavior of Plasma Sprayed Segmented Thermal Barrier Coatings. Materials Transactions, 2006, 47, 306-309.	0.4	40
49	High-temperature oxidation behavior of β-NiAl with various reactive element dopants in dry and humid atmospheres. Corrosion Science, 2014, 83, 335-342.	3.0	40
50	Interdiffusion behavior between NiAlHf coating and Ni-based single crystal superalloy with different crystal orientations. Applied Surface Science, 2015, 326, 124-130.	3.1	40
51	Phase stability and thermal conductivity of ytterbia and yttria co-doped zirconia. Progress in Natural Science: Materials International, 2013, 23, 440-445.	1.8	39
52	Effects of Dy on the adherence of Al2O3/NiAl interface: A combined first-principles and experimental studies. Corrosion Science, 2013, 66, 59-66.	3.0	39
53	Effect of thermal exposure on the microstructure and properties of EB-PVD gradient thermal barrier coatings. Surface and Coatings Technology, 2003, 168, 23-29.	2.2	38
54	Microstructure evolution of an EB-PVD NiAl coating and its underlying single crystal superalloy substrate. Journal of Alloys and Compounds, 2016, 672, 36-44.	2.8	38

#	Article	IF	CITATIONS
55	Impact interaction of in-flight high-energy molten volcanic ash droplets with jet engines. Acta Materialia, 2019, 171, 119-131.	3.8	37
56	The role of Cr and Si in affecting high-temperature oxidation behaviour of minor Dy doped NiAl alloys. Corrosion Science, 2013, 77, 322-333.	3.0	36
57	Synergistic effect of reactive element co-doping in two-phase (γ' + β) Ni-Al alloys. Corrosion Science, 2017, 120, 130-138.	3.0	36
58	Effects of Dy on cyclic oxidation resistance of NiAl alloy. Transactions of Nonferrous Metals Society of China, 2009, 19, 1185-1189.	1.7	35
59	Cyclic oxidation behavior of Hf/Zr co-doped EB-PVD β-NiAl coatings at 1200 °C. Surface and Coatings Technology, 2015, 276, 721-725.	2.2	35
60	Novel microstructure of EB-PVD double ceramic layered thermal barrier coatings. Thin Solid Films, 2008, 516, 5736-5739.	0.8	34
61	Effect of Ru on interdiffusion dynamics of β-NiAl/DD6 system: A combined experimental and first-principles studies. Materials and Design, 2015, 88, 667-674.	3.3	34
62	Improved alumina scale adhesion of electron beam physical vapor deposited Dy/Hf-doped β-NiAl coatings. Applied Surface Science, 2013, 283, 513-520.	3.1	33
63	Microstructures and deposition mechanisms of quasi-columnar structured yttria-stabilized zirconia coatings by plasma spray physical vapor deposition. Ceramics International, 2017, 43, 12920-12929.	2.3	33
64	Thermal cycling behavior of (Gd0.9Yb0.1)2Zr2O7/8YSZ gradient thermal barrier coatings deposited on Hf-doped NiAl bond coat by EB-PVD. Surface and Coatings Technology, 2014, 258, 950-955.	2.2	31
65	Tightly adhered silk fibroin coatings on Ti6Al4V biometals for improved wettability and compatible mechanical properties. Materials and Design, 2019, 175, 107825.	3.3	31
66	Ruddlesden–Popper structured BaLa2Ti3O10, a highly anisotropic material for thermal barrier coatings. Ceramics International, 2012, 38, 4345-4352.	2.3	30
67	Oxidation and microstructure evolution of Al–Si coated Ni3Al based single crystal superalloy with high Mo content. Applied Surface Science, 2015, 325, 20-26.	3.1	30
68	Effect of Y doping on microstructure and thermophysical properties of yttria stabilized hafnia ceramics. Ceramics International, 2018, 44, 18213-18221.	2.3	30
69	Thermal barrier coating bonded by (Al2O3–Y2O3)/(Y2O3-stabilized ZrO2) laminated composite coating prepared by two-step cyclic spray pyrolysis. Corrosion Science, 2014, 80, 37-45.	3.0	28
70	Fabrication of WCp/NiBSi metal matrix composite by electron beam melting. Materials Science & Engineering A: Structural Materials: Properties, Microstructure and Processing, 2016, 666, 320-323.	2.6	28
71	Oxidation and diffusion barrier behaviors of double-layer NiCoCrAlY coatings produced by plasma activated EB-PVD. Surface and Coatings Technology, 2011, 205, 4658-4664.	2.2	27
72	The influence of Gd doping on thermophysical properties, elasticity modulus and phase stability of garnet-type (Y1-Gd)3Al5O12 ceramics. Journal of the European Ceramic Society, 2017, 37, 4171-4177.	2.8	27

#	Article	IF	CITATIONS
73	Effects of Yb3+ doping on phase structure, thermal conductivity and fracture toughness of (Nd1-xYbx)2Zr2O7. Ceramics International, 2019, 45, 3133-3139.	2.3	27
74	Effects of Heat Treatment on Microstructures and Physical Properties of Segmented Thermal Barrier Coatings. Materials Transactions, 2005, 46, 1775-1778.	0.4	26
75	Effect of water vapor on the phase transformation of alumina grown on NiAl at 950°C. Corrosion Science, 2011, 53, 2943-2947.	3.0	26
76	Synthesis, thermal conductivities and phase stability of Gd3TaO7 and La doped Gd3TaO7 ceramics. Journal of Alloys and Compounds, 2018, 732, 759-764.	2.8	26
77	Preparation of Al2O3–YSZ composite coating by EB-PVD. Materials Science & Engineering A: Structural Materials: Properties, Microstructure and Processing, 2002, 325, 389-393.	2.6	25
78	Microstructure of oxides in thermal barrier coatings grown under dry/humid atmosphere. Corrosion Science, 2011, 53, 2630-2635.	3.0	25
79	The formation mechanisms of HfO2 located in different positions of oxide scales on ni-al alloys. Corrosion Science, 2020, 167, 108481.	3.0	25
80	Evaluation of hot-fatigue behaviors of EB-PVD gradient thermal barrier coatings. Materials Science & Engineering A: Structural Materials: Properties, Microstructure and Processing, 2002, 325, 261-269.	2.6	24
81	Thermal barrier coatings with (Al2O3–Y2O3)/(Pt or Pt–Au) composite bond coat and 8YSZ top coat on Ni-based superalloy. Applied Surface Science, 2013, 286, 298-305.	3.1	24
82	Microstructures of La2Ce2O7 coatings produced by plasma spray-physical vapor deposition. Journal of the European Ceramic Society, 2020, 40, 1462-1470.	2.8	23
83	Dynamic spreading of re-melted volcanic ash bead on thermal barrier coatings. Corrosion Science, 2020, 170, 108659.	3.0	23
84	Improved oxidation resistance and diffusion barrier behaviors of gradient oxide dispersed NiCoCrAlY coatings on superalloy. Vacuum, 2010, 85, 627-633.	1.6	22
85	Effect of thermal cycling on microstructure evolution and elements diffusion behavior near the interface of Ni/NiAl diffusion couple. Journal of Alloys and Compounds, 2015, 642, 117-123.	2.8	22
86	PS-PVD gadolinium zirconate thermal barrier coatings with columnar microstructure sprayed from sintered powder feedstocks. Surface and Coatings Technology, 2020, 383, 125243.	2.2	22
87	CYCLIC OXIDATION BEHAVIORS OF EB-PVD Dy DOPED β- NiAl COATINGS AT 1100°C. International Journal of Modern Physics B, 2010, 24, 3143-3148.	1.0	21
88	Microstructural evolution of CoCrAlY bond coat on Ni-based superalloy DZ 125 at 1050°C. Surface and Coatings Technology, 2011, 205, 4374-4379.	2.2	21
89	The ordering degree and thermal conductivity in the pyrochlore-type composition systems with a constant cation radius ratio. Materials Letters, 2013, 106, 119-121.	1.3	21
90	Improved oxide scale adherence of low-Pt/Hf co-doped β-NiAlCrSi coating on superalloy IC21 at 1200°C. Corrosion Science, 2016, 105, 78-87.	3.0	21

#	Article	IF	CITATIONS
91	Evolution mechanism of the microstructure and mechanical properties of plasma-sprayed yttria-stabilized hafnia thermal barrier coating at 1400°C. Ceramics International, 2020, 46, 23417-23426.	2.3	21
92	The phase stability and thermophysical properties of InFeO3(ZnO)m (m=2, 3, 4, 5). Journal of the European Ceramic Society, 2014, 34, 63-68.	2.8	20
93	Self-toughening behavior of nano yttria partially stabilized hafnia ceramics. Ceramics International, 2019, 45, 21467-21474.	2.3	20
94	Microstructure and high-temperature oxidation behavior of plasma-sprayed Si/Yb2SiO5 environmental barrier coatings. Chinese Journal of Aeronautics, 2019, 32, 1994-1999.	2.8	20
95	Evaluation of stress distribution and failure mechanism in lanthanum–titanium–aluminum oxides thermal barrier coatings. Ceramics International, 2013, 39, 5103-5111.	2.3	19
96	Sintering of electron beam physical vapor deposited thermal barrier coatings under flame shock. Ceramics International, 2013, 39, 5093-5102.	2.3	19
97	The residual stress of oxide scales grown on Ni-Al alloys doped with minor Dy and Y. Corrosion Science, 2016, 112, 542-551.	3.0	19
98	Microstructural Degradation of Ti-45Al-8Nb Alloy During the Fabrication Process by Electron Beam Melting. Jom, 2017, 69, 2596-2601.	0.9	19
99	Microstructural evolution of plasma spray physical vapor deposited thermal barrier coatings at 1150â∈ °C studied by impedance spectroscopy. Ceramics International, 2018, 44, 10797-10805.	2.3	18
100	Investigation of the thermophysical properties of (Y1-xYbx)TaO4 ceramics. Journal of the European Ceramic Society, 2020, 40, 3111-3121.	2.8	18
101	Reactive elements dependence of elastic properties and stacking fault energies of γ-Ni, γ′-Ni3Al and β-NiAl. Journal of Alloys and Compounds, 2020, 843, 155799.	2.8	18
102	Surface roughness affects metastable non-wetting behavior of silicate melts on thermal barrier coatings. Rare Metals, 2022, 41, 469-481.	3.6	18
103	Influence of Yb 3+ doping on phase stability and thermophysical properties of (Y 1-x Yb x) 3 Al 5 O 12 under high temperature. Ceramics International, 2017, 43, 7153-7158.	2.3	17
104	Impermeability of Y3Al5O12 ceramic against molten glassy calcium-magnesium-alumina-silicate. Chinese Journal of Aeronautics, 2018, 31, 2306-2311.	2.8	17
105	Mechanical properties and thermal conductivities of 3YSZ-toughened fully stabilized HfO2 ceramics. Ceramics International, 2019, 45, 12851-12859.	2.3	17
106	Microscale lamellar NiCoCrAlY coating with improved oxidation resistance. Surface and Coatings Technology, 2012, 207, 110-116.	2.2	16
107	Cyclic Oxidation Behavior of an EB-PVD CoCrAlY Coating Influenced by Substrate/coating Interdiffusion. Chinese Journal of Aeronautics, 2012, 25, 796-803.	2.8	16
108	Phase stability, microstructural and thermo-physical properties of BaLn 2 Ti 3 O 10 (Ln=Nd and Sm) ceramics. Ceramics International, 2013, 39, 6743-6749.	2.3	16

#	Article	IF	CITATIONS
109	Improved hot-corrosion resistance of Si/Cr co-doped NiAlDy alloy in simulative sea-based engine environment. Corrosion Science, 2014, 85, 232-240.	3.0	16
110	Microstructure and cyclic oxidation behaviour of low-Pt/Dy co-doped β-NiAl coatings on single crystal (SC) superalloy. Surface and Coatings Technology, 2016, 304, 108-116.	2.2	16
111	EFFECTS OF Dy ON THE MICROSTRUCTURE AND SPALLATION FAILURE OF THE ALUMINA SCALES GROWN ON NiAl . International Journal of Modern Physics B, 2010, 24, 3149-3154.	1.0	15
112	Microstructures and mechanical properties of β-NiAlHf coated single crystal superalloy. Materials Science & Engineering A: Structural Materials: Properties, Microstructure and Processing, 2016, 673, 39-46.	2.6	15
113	Novel Prospects for Plasma Spray–Physical Vapor Deposition of Columnar Thermal Barrier Coatings. Journal of Thermal Spray Technology, 2017, 26, 1810-1822.	1.6	15
114	Impact of Si addition on high-temperature oxidation behavior of NiAlHf alloys. Journal of Materials Science and Technology, 2019, 35, 2038-2047.	5.6	15
115	Corrosion resistant plasma sprayed (Y0.8Gd0.2)3Al5O12/YSZ thermal barrier coatings towards molten calcium-magnesium-alumina-silicate. Ceramics International, 2019, 45, 8138-8144.	2.3	15
116	Effect of splat-interface discontinuity on effective thermal conductivity of plasma sprayed thermal barrier coating. Ceramics International, 2020, 46, 4824-4831.	2.3	15
117	Hot corrosion behavior of NdYbZr2O7 exposed to V2O5 and Na2SO4 + V2O5 molten salts. Ceramics International, 2020, 46, 8543-8552.	2.3	15
118	Thermo-physical and mechanical properties of Yb2O3 and Sc2O3 co-doped Gd2Zr2O7 ceramics. Ceramics International, 2020, 46, 18888-18894.	2.3	15
119	Plasma–Powder Feedstock Interaction During Plasma Spray–Physical Vapor Deposition. Journal of Thermal Spray Technology, 2017, 26, 292-301.	1.6	14
120	High-temperature CMAS resistance performance of Ti2AlC oxide scales. Corrosion Science, 2020, 174, 108832.	3.0	14
121	Improved fracture toughness and multiple toughening mechanisms of NdPO4/NdYbZr2O7 composites. Ceramics International, 2020, 46, 16612-16619.	2.3	14
122	Effects of Dy on Transient Oxidation Behavior of EB-PVD β-NiAl Coatings at Elevated Temperatures. Chinese Journal of Aeronautics, 2011, 24, 363-368.	2.8	13
123	Cyclic oxidation and interdiffusion behavior of Pt modified NiAlHfCrSi coatings on single crystal superalloy containing Mo. Surface and Coatings Technology, 2014, 259, 426-433.	2.2	13
124	Effect of different B contents on the mechanical properties and cyclic oxidation behaviour of β-NiAlDy coatings. Journal of Alloys and Compounds, 2015, 623, 83-88.	2.8	13
125	Oxidation behaviour of electron beam physical vapour deposition β-NiAlHf coatings at 1100°C in dry and humid atmospheres. Rare Metals, 2016, 35, 513-519.	3.6	13
126	Deposition mechanisms of columnar structured La2Ce2O7 coatings via plasma spray-PVD. Ceramics International, 2020, 46, 13424-13432.	2.3	13

#	Article	IF	CITATIONS
127	Effects of rare earth oxides on microstructures and thermo-physical properties of hafnia ceramics. Journal of Materials Science and Technology, 2021, 72, 144-153.	5.6	13
128	PS–PVD Alumina Overlayer on Thermal Barrier Coatings Against CMAS Attack. Journal of Thermal Spray Technology, 2021, 30, 864-872.	1.6	13
129	Microstructure, mechanical and corrosion properties of electron-beam-melted and plasma-transferred arc-welded WCP/NiBSi metal matrix composites. Rare Metals, 2019, 38, 814-823.	3.6	12
130	Novel thermal barrier coatings with hexagonal boron nitride additives resistant to molten volcanic ash wetting. Corrosion Science, 2020, 168, 108587.	3.0	12
131	Microstructures and Phases of Ytterbium Silicate Coatings Prepared by Plasma Spray-Physical Vapor Deposition. Materials, 2020, 13, 1721.	1.3	12
132	Silicate ash-resistant novel thermal barrier coatings in gas turbines. Corrosion Science, 2022, 194, 109929.	3.0	12
133	Numerical analysis of the plasma-induced self-shadowing effect of impinging particles and phase transformation in a novel long laminar plasma jet. Journal Physics D: Applied Physics, 2020, 53, 375202.	1.3	11
134	Cyclic oxidation behavior of β-NiAlDy alloys containing varying aluminum content at 1200°C. Progress in Natural Science: Materials International, 2012, 22, 311-317.	1.8	10
135	Thermal deformation of Y2O3 partially stabilized ZrO2 coatings by digital image correlation method. Surface and Coatings Technology, 2013, 216, 1-7.	2.2	10
136	Title is missing!. Journal of Materials Science, 2002, 37, 5333-5337.	1.7	9
137	Failure mechanism of EB-PVD thermal barrier coatings on NiAl substrate. Transactions of Nonferrous Metals Society of China, 2007, 17, 811-815.	1.7	9
138	Impedance spectroscopy study of high-temperature oxidation of Gd2O3-Yb2O3 codoped zirconia thermal barrier coatings. Transactions of Nonferrous Metals Society of China, 2011, 21, 1061-1067.	1.7	9
139	Effects of Pressure during Preparation on the Grain Orientation of Ruddlesden–Popper Structured BaLa2Ti3O10 Ceramic. Journal of Materials Science and Technology, 2014, 30, 455-458.	5.6	9
140	Evolution mechanism of interface cohesion for the coating inducing by laser cladding YSZ@Ni core-shell nanoparticles: Experimental and theoretical research. Journal of Alloys and Compounds, 2017, 708, 844-852.	2.8	9
141	Deposition of TiN by plasma activated EB-PVD: Activation by thermal electron emission from molten niobium. Surface and Coatings Technology, 2015, 276, 645-648.	2.2	8
142	Deposition of TiN/TiAlN multilayers by plasma-activated EB-PVD: tailored microstructure by jumping beam technology. Rare Metals, 2017, 36, 651-658.	3.6	8
143	Microstructural evolution, mechanical properties and degradation mechanism of PS-PVD quasi-columnar thermal barrier coatings exposed to glassy CMAS deposits. Rare Metals, 0, , 1.	3.6	8
144	Microstructure Dependence of Effective Thermal Conductivity of EB-PVD TBCs. Materials, 2021, 14, 1838.	1.3	8

#	Article	IF	CITATIONS
145	Improved thermal barrier properties of InFeZnO4 ceramics by Gd/Yb doping. Journal of Alloys and Compounds, 2014, 585, 404-406.	2.8	7
146	Isothermal Oxidation Behavior of Dysprosium/S-Doped β-NiAl Alloys at 1200°C. Journal of Materials Science and Technology, 2014, 30, 229-233.	5.6	7
147	Microstructure stability of γâ€2Â+ÂÎ2 Ni–Al coated single-crystal superalloy N5 annealed at 1100°C. Rare Metals, 2021, 40, 693-700.	3.6	7
148	Thermal cycling performance of La2Ce2O7/YSZ TBCs with Pt/Dy co-doped NiAl bond coat on single crystal superalloy. Rare Metals, 2021, 40, 2568-2578.	3.6	7
149	Cyclic oxidation behavior of Cr-/Si-modified NiAlHf coatings on single-crystal superalloy produced by EB-PVD. Rare Metals, 2016, 35, 396-400.	3.6	6
150	Silk Lattice Structures from Unidirectional Silk Fiber–Reinforced Composites for Breaking Energy Absorption. Advanced Engineering Materials, 2020, 22, 1900921.	1.6	6
151	Mechanical Properties and Thermal Conductivity of Ytterbium-Silicate-Mullite Composites. Materials, 2020, 13, 671.	1.3	6
152	Novel long laminar plasma sprayed hybrid structure thermal barrier coatings for high-temperature anti-sintering and volcanic ash corrosion resistance. Journal of Materials Science and Technology, 2021, 79, 141-146.	5.6	6
153	Prediction of Thermal Conductivity of Composite Materials. Journal of Power and Energy Systems, 2008, 2, 1048-1059.	0.5	5
154	Thermal transport properties of InFeZnO4–YbFeZnO4 solid solutions. Journal of Alloys and Compounds, 2015, 623, 203-208.	2.8	5
155	Processing and oxidation behavior of Pt-diffused coatings. Rare Metals, 2020, 39, 902-908.	3.6	5
156	Measurements of the thermal gradient over EB-PVD thermal barrier coatings. Vacuum, 2003, 70, 11-16.	1.6	4
157	Cyclic oxidation behavior of electron beam physical vapor deposition NiAlHf and NiAlHfCrSi coatings at 1150°C. Rare Metals, 2023, 42, 1408-1413.	3.6	4
158	Correlation of Feedstock Powder Characteristics with Microstructure, Composition, and Mechanical Properties of La2Ce2O7 Coatings Produced by Plasma Spray-Physical Vapor Deposition. Coatings, 2020, 10, 93.	1.2	4
159	Internal Factors Affecting the Surface Rumpling of a \hat{I}^2 -NiAlHf Coating. Coatings, 2021, 11, 436.	1.2	4
160	INTER-DIFFUSION BEHAVIOR OF RECOATED CoCrAlY COATING/DZ125 DIRECTIONALLY SOLIDIFIED SUPERALLOY. Jinshu Xuebao/Acta Metallurgica Sinica, 2013, 49, 229.	0.3	4
161	High-temperature oxidation behaviour of minor Hf-doped β-NiAl single crystals in dry and humid atmospheres. Rare Metals, 2023, 42, 2767-2773.	3.6	3
162	Existence patterns of Dy in Î ² -NiAl from first-principles calculations. Rare Metals, 2016, 35, 356-360.	3.6	2

#	Article	IF	CITATIONS
163	Plasma characteristics and coating microstructures of yttria stabilized zirconia during plasma spray physical vapor deposition. , 2017, , .		2
164	Sub-micron Co–Al2O3 composite powders prepared by room-temperature ultrasonic-assisted electroless plating. Rare Metals, 2015, , 1.	3.6	1
165	Plasma flow optimization for 7YSZ quasi-columnar coating by plasma spray-physical vapor deposition. , 2018, , .		1
166	Processing of a low-cost γ–γ′ NiPtAl coating with improved oxidation resistance. Rare Metals, 0, , 1.	3.6	1
167	HOT-CORROSION BEHAVIOR OF THERMAL BARRIER COATED DZ125 SUPERALLOY EXPOSED TO ATOMIZED SEAWATER AND KEROSENE. International Journal of Modern Physics B, 2010, 24, 3155-3160.	1.0	0
168	High-temperature oxidation resistance of Si-coated C/SiC composites. Rare Metals, 2019, , 1.	3.6	0
169	Surface Rumpling Behavior of Hf/Zr Single-Doped and Co-Doped β-NiAl Coatings during High-Temperature Cyclic Oxidation. Coatings, 2020, 10, 874.	1.2	0